Hindawi Publishing Corporation
Journal of Nanomaterials
Volume 2014, Article ID 105875, 10 pages
http://dx.doi.org/10.1155/2014/105875

Research Article

Synthesis of ZnO Nanowires via Hotwire Thermal Evaporation of Brass (CuZn) Assisted by Vapor Phase Transport of Methanol

Tamil Many K. Thandavan,[1] Siti Meriam Abdul Gani,[2] Chiow San Wong,[1] and Roslan Md Nor[1]

[1] *Plasma Technology Research Centre, Department of Physics, University of Malaya, Lembah Pantai, 50603 Kuala Lumpur, Malaysia*
[2] *Low Dimensional Material Research Centre, Department of Physics, University of Malaya, Lembah Pantai, 50603 Kuala Lumpur, Malaysia*

Correspondence should be addressed to Tamil Many K. Thandavan; tamilmanykthandavan@gmail.com and Roslan Md Nor; rmdnor@um.edu.my

Received 20 March 2014; Revised 14 May 2014; Accepted 15 May 2014; Published 18 June 2014

Academic Editor: Benxia Li

Zinc oxide (ZnO) nanowires (NWs) were synthesized using vapor phase transport (VPT) and thermal evaporation of Zn from CuZn. Time dependence of ZnO NWs growth was investigated for 5, 10, 15, 20, 25, and 30 minutes. Significant changes were observed from the field electron scanning electron microscopy (FESEM) images as well as from the X-ray diffraction (XRD) profile. The photoluminescence (PL) profile was attributed to the contribution of oxygen vacancy, zinc interstitials, and hydrogen defects in the ZnO NWs. Raman scattering results show a significant peak at 143 cm^{-1} and possible functionalization on the wall of ZnO NWs. Growth of ZnO NWs in (0002) with an estimated distance between adjacent lattice planes 0.26 nm was determined from transmission electron microscopy (TEM) analysis.

1. Introduction

ZnO is a unique material with a wide band gap of 3.37 eV and a large exciton binding energy of 60 meV at room temperature. These properties and the development of nanosized ZnO have attracted much attention both in basic science and industrial applications [1]. Thus, many efforts have been employed for achieving ZnO in one-dimensional (1D) nanostructures as nanotubes [2], nanowires [3], nanorods [4, 5], nanobelts [6], nanocables [7], and nanoribbons [8] using physical evaporization [9], chemical vapor deposition [10, 11], solvothermal [12], and carbothermal method [13] on different substrate materials. However, the growth techniques are ranged from low temperature wet chemical growth technique to metal organic chemical vapor deposition (MOCVD) technique [14] at temperatures above 1000°C. The MOCVD technique has led to high quality growth of columnar structured film with higher growth rate but not straight forward to fabricate smooth ZnO thin film on flat surfaces. Indeed, growing ZnO film homoepitaxially on ZnO substrate using vapor phase transport (VPT) method [15] was favored earlier but seems to be far from cost-effective and high volume production. Nevertheless, VPT is still a suitable technique to grow nanoscale ZnO NWs in bulk, nanorods, and thin film effectively since this method allows NWs to be grown directly from substrate and does not require any catalyst or seed layers to promote the growth of ZnO NWs [16]. Apart from this, VPT enables the control of morphology and size of the nanostructures as parameters like reaction time and temperature are adjustable. Yu et al. have reported that reaction time less than 2 hours has produced high quality ZnO NWs via VPT compared to organic solution based chemistry which takes about 2 to 12 h [16]. Earlier, Zhu et al [17]. used VPT method and detailed a comparative study on ZnO NWs growth using different metal catalyst and different substrate material. This has imparted

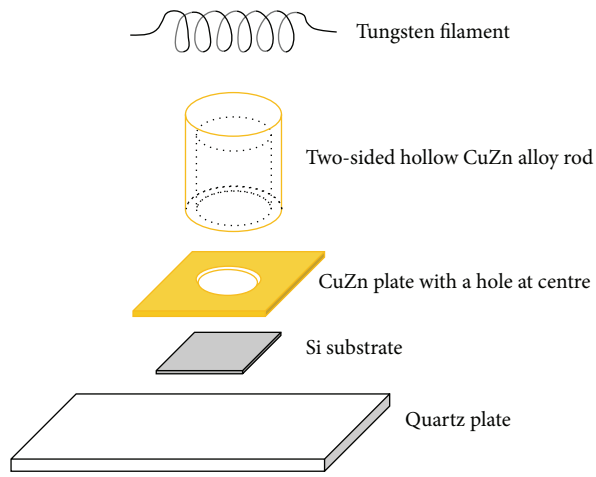

Figure 1: Illustration of experimental setup in order from bottom; quartz plate, Si substrate, CuZn plate, two-sided hollow CuZn metal rod, and tungsten hotwire in a vacuum chamber.

one-dimensional ZnO nanostructures with different range of diameters, densities, and aspect ratios [17]. In this study we are reporting a technique that consumes deposition period and is feasible in growing ZnO at suitable temperature on silicon substrate. This involves the combination of VPT of methanol and thermal evaporation of CuZn to obtain large area of deposition with reduced time of reaction. The use of CuZn as the Zn source is to benefit from a solid source with the potential to be fashioned to produce patterned deposition. The technique described here is significantly different from other reported techniques of the synthesis of ZnO nanostructures directly on Zn substrates or using mixtures of ZnO and carbon powders. With CuZn, the dezincification process [18] where Zn segregates to the surface of CuZn when heated to below its melting point of 914°C is utilized. The Zn droplets formed during the dezincification process are transported to the substrate surface under gas flow to be oxidized to ZnO.

2. Experimental

The ZnO NWs were grown on Si (001) substrate. CuZn alloy was used as Zn source, whereas methanol was used as source of oxygen in this work. CuZn alloy of 55.11, 37.91, 3.84, and 3.13 weight % for Cu, Zn, Al, and Pb, respectively, was verified by EDAX measurement and was used as Zn source. Mirror finished Si (001) wafer was used as a substrate for the growth of ZnO NWs. The Si wafer was cut into chips about 1.5 by 1.5 cm and the oxide layer removed using hydrofluoric acid (HF) solution. Then the Si chips were cleaned ultrasonically about 30 minutes in acetone solution. The cleaned Si chips were rinsed in deionized (DI) water and let to dry in desiccators at room temperature to remove moisture content on the Si substrate. The dried Si chip was placed on a quartz slide before being transferred into the vacuum chamber. A CuZn alloy plate thickness of 0.5 mm with dimension of 2.3 by 2.3 cm and 0.5 cm diameter hole in middle was cleaned ultrasonically in acetone bath and rinsed with DI water before placing it on the Si chip. A two-sided hollow CuZn rod was placed on the Si chip to cover the whole surface of Si substrate. The illustration of experimental setup is shown in Figure 1.

Argon (Ar) was flowed at 100 sccm through mixture of methanol and acetone solution to allow methanol vapor to be transported into the deposition chamber. The gas tubing systems were filled with drying agent and potassium silicates in order to allow dried methanol and Ar flow into the deposition chamber. This methanol vapor underwent thermal dissociation under tungsten hotwire which was heated to 1800°C. Copper (Cu) in the CuZn did not undergo thermal evaporation due to its higher melting point compared to the operating temperature. Zn in CuZn was thermally evaporated at temperature greater than 395°C. The vaporized Zn and methanol particles were condensed on Si substrate which was monitored at temperature of 800°C. The deposition period was prolonged for 30 minutes. At the end of the 30th minute the methanol transportation was halted and the hotwire was switched off but continuous flow of Ar at 100 sccm without flowing through the mixture of methanol and acetone solution was maintained until the temperature of substrate dropped to room temperature. The influence of growth time dependent of ZnO NWs was investigated by varying the growth time periods to 25, 20, 15, 10, and 5 minutes.

3. Results and Discussions

3.1. FESEM. Figure 2 shows the images of ZnO NWs prepared at various growth times of 5, 10, 15, 20, 25, and 30 minutes. Significant changes in the morphology and structure of ZnO NWs are identical as the growth time was varied. Growth of hexagonal nanorods and NWs is observable as displayed in Figure 2. The stem can be attributed to hexagonal wurtzite ZnO structure which stacks up to a button shaped ZnO.

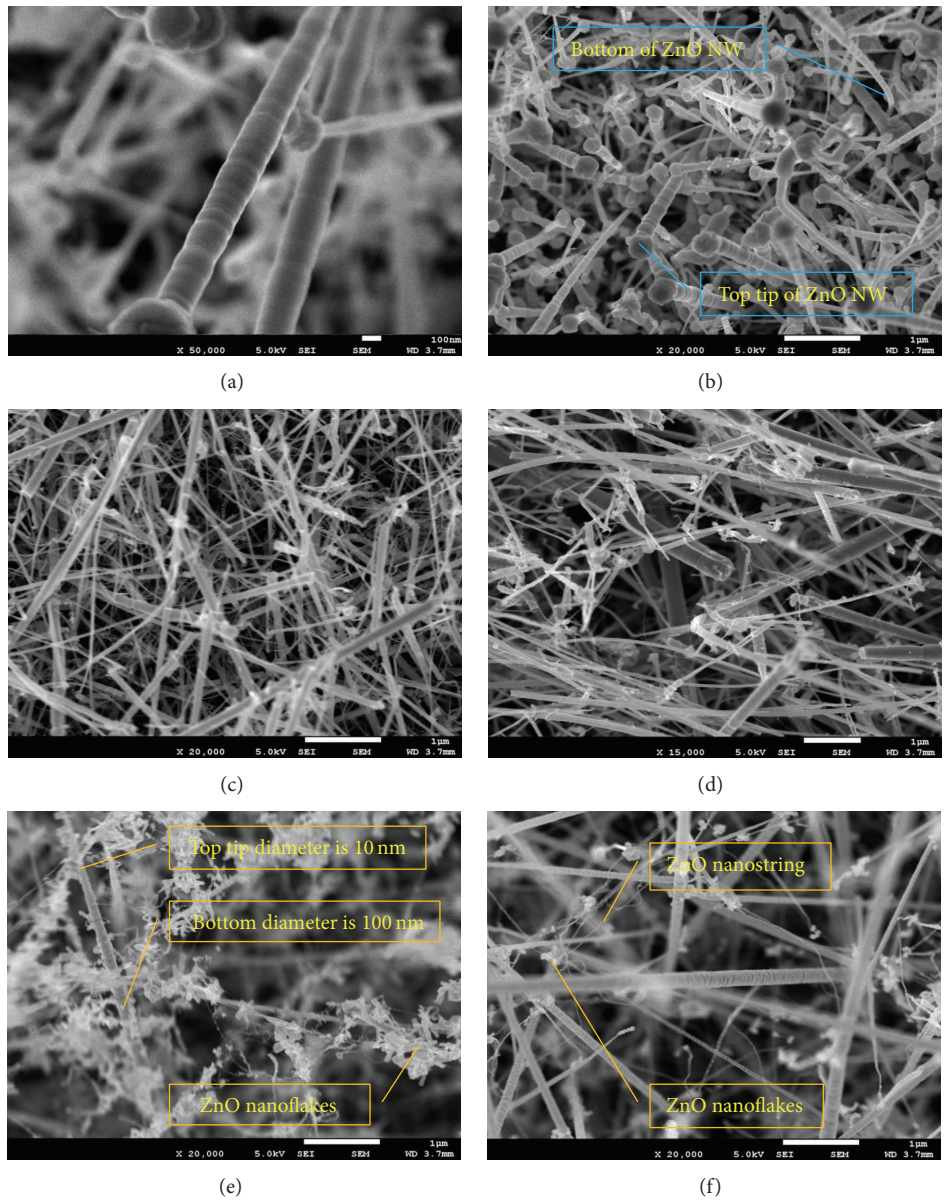

Figure 2: Images (a), (b), (c), (d), (e), and (f) are ZnO NWs prepared at deposition times of 5, 10, 15, 20, 25, and 30 minutes.

At growth times of 5 and 10 minutes, growth like button mushrooms are observable as shown in Figures 2(a) and 2(b). The diameters of the NWs ranged from 10 nm at the bottom to few hundred nm to the top tip and seem to be stacks of hexagonal ZnO plates in a single NW. The stacked hexagonal shape ZnO NWs are randomly orientated in long and straight dimension in whole direction on the Si substrate as seen in Figures 2(a) and 2(b).

Figures 2(c) and 2(d) are images of ZnO NWs produced for growth time of 15 and 20 minutes. They are also randomly orientated as long and straight NWs on Si substrate. The lengths are observed to be up to few microns greater than ZnO NWs prepared at growth times of 5 and 10 minutes. Their diameters ranged from 10 to 100 nm. Besides that, formations of ZnO flakes are also observable in the ZnO NWs prepared at growth time of 20 minutes which could be an initial stage of formation of ZnO nanoflakes. More ZnO nanoflakes were observed to be around the NWs at growth times of 25 and 30 minutes. Tiny nanostrings also were grown connecting the ZnO nanoflakes as seen in Figure 2(f). However, the diameters ranged from 100 nm at the bottom to 10 nm to the top tip which looks like nanoneedles. This growth shape of ZnO nanoneedles is in opposition of ZnO NWs of 5 and 10 minutes growth time.

3.2. XRD. Figure 3 shows the XRD spectra of growth time-dependent for ZnO NWs deposited on Si substrate in 5, 10, 15, 20, 25, and 30 minutes. The diffracted peaks attribute the polycrystalline nature of ZnO which can be indexed to the hexagonal wurtzite type ZnO (JCP2.2CA: 00-036-1451).

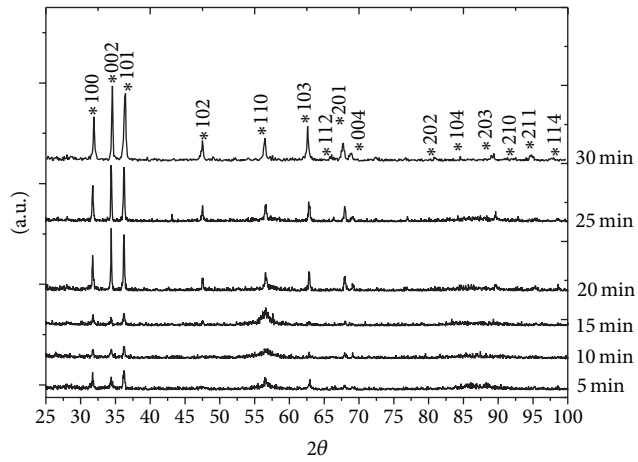

Figure 3: XRD spectra of ZnO NWs prepared at growth times of 5, 10, 15, 20, 25, and 30 minutes are stacked up.

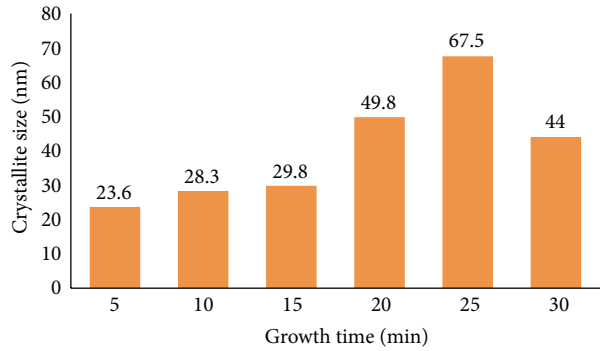

Figure 4: Crystallite size of ZnO/methanol NWs obtained at growth times of 5, 10, 15, 20, 25, and 30 minutes.

The prevalence of the peak that corresponds to (100) and (101) directions points to a preferential deposition time of 5, 10, and 15 minutes, whereas preferential growth direction in (002) plane is observable for growth times of 20, 25, and 30 minutes. This may be due to the fact that there are no enough energized particles in the beginning of 5 to 15 minutes to move to low-energy sites that induced strain in the film. Significant contribution in the (100), (002), and (101) direction are noticeable when the deposition time is increased from 20 to 30 minutes but very slight preferential orientation is noticed in ⟨002⟩ direction. This renders that more energized particles occupied the low energy sites in c-axis direction. Based on the preferential growth direction (002) with the increased deposition time, crystallite size (D) of ZnO is calculated using Scherer formula [19]. The peak center of (002) from Gaussian deconvoluted shows slight shift to the left compared to the standard peak center 2θ of 34.422 of bulk ZnO (5.20661 Å). This indicates uniform tensile stress is distributed with higher calculated d spacing value of 2.604 Å.

Table 1 shows that the calculated crystallite size has increased as the growth time was increased. Figure 4 shows distribution of crystallite size at growth times of 5 to 30 minutes. The crystallite size found to be increased at low rate during the growth time of 5, 10, and 15 minutes which could be due to formation of low energy site of lattice ZnO. During 20, 25, and 30 minutes of growth time, the crystallite size dramatically increased to 49.8, 67.5, and 44.0 nm, respectively. This could be condensation of energized particles such as O species onto the low energy site of ZnO. At higher growth time, the density of growth of ZnO might have increased which could be due to condensation of more energized particles into NWs. The percentage of increment of crystallite size of ZnO NWs is worked out for an increased deposition time of 5 minutes as shown below

$$\begin{array}{ll} \text{increment of crystallie size:} & 17\% \quad 5\% \quad 40\% \quad 35\% \quad -34\% \\ \text{Deposition time:} & 5 \longrightarrow 10 \longrightarrow 15 \longrightarrow 20 \longrightarrow 25 \longrightarrow 30. \end{array} \tag{1}$$

Table 1: Details of ZnO NWs deposited at growth times of 5, 10, 15, 20, 25, and 30 minutes.

Deposition time (minutes)	Peak center (2θ) (002)	Crystallite size, D (nm)	d spacing (Å)		Lattice parameter (Å)		Ratio c/a	Volume (nm^3)
			(002)	(101)	a	c		
5	34.388	23.6	2.60482	2.47700	3.25102	5.20960	1.6025	47.68
10	34.380	28.3	2.60528	2.47562	3.24865	5.21082	1.6040	47.63
15	34.390	29.8	2.60432	2.47619	3.24990	5.20933	1.6029	47.65
20	34.393	49.8	2.60449	2.47642	3.25039	5.20893	1.6026	47.64
25	34.396	67.5	2.60400	2.47684	3.25111	5.20846	1.6021	47.68
30	34.387	44.0	2.60486	2.47667	3.25063	5.20972	1.6027	47.67

We believe that high percentages of increment 17%, 40%, 35%, and 34% are identified for the increment of 5 minutes of deposition time from 5 to 10 minutes, 15 to 20 minutes, 20 to 25 minutes, and 25 to 30 minutes. This is due to the more energized particles that have occupied the low energy sites of the lattice of ZnO NWs, whereas low percentage of 5% for the increment of 5 minutes of deposition time from 10 to 15 minutes indicates that not enough energized particles occupied the lattice of ZnO NWs. The discernible change of growth percentage of ZnO NWs explicates a sinusoidal growth trend whereby creation and occupancy of low energy sites simultaneously have taken place for each increment of 5 minutes deposition time. However, optimization in the growth time is noticed after 25 minutes of deposition.

3.3. Photoluminescence. PL study was carried out using Renishaw inVia Raman microscope at room temperature in the wavelength range from 350 to 800 nm using a 325 nm helium-cadmium (He-Cd) laser light which passes through three visible lens sets and a diffraction grating of 1200 lines/mm. The respective PL profile for ZnO NWs prepared at various growth times of 5, 10, 15, 20, 25, and 30 minutes is shown in Figure 5. It is generally accepted that the surface states play a crucial role in PL spectra of ZnO nanomaterials [20]. Energy transition within the ZnO NWs and relationship between material color and defect structure were determined. The normalized PL shows a low near band-edge (NBE) emissions at ~382 nm, deep level (DL) emissions at ~540 nm, and near infrared (NIR) emissions at ~765 nm for all the samples.

Figure 5 also indicates that the intensity of the emissions has decreased as the growth time was increased. The increased integral intensity of NBE emission indicates significant changes in the crystallinity of ZnO NWs as well as the diameter of the NWs [21]. High crystallinity of ZnO is related to decrease of impurities and structural defects such as oxygen vacancy (Vo) and dislocations [22]. The decreased NBE also indicates rapid recombination of charge carriers in the defect energy states, which gives rise to intense DL emission as observed in Figure 5. The dependence of this DL emission on the growth times was analyzed to investigate the defect structure in ZnO. In order to compare the relative contributions to the emissions Gaussian deconvoluted peaks were obtained for NBE, DL, and NIR and detailed in Table 2.

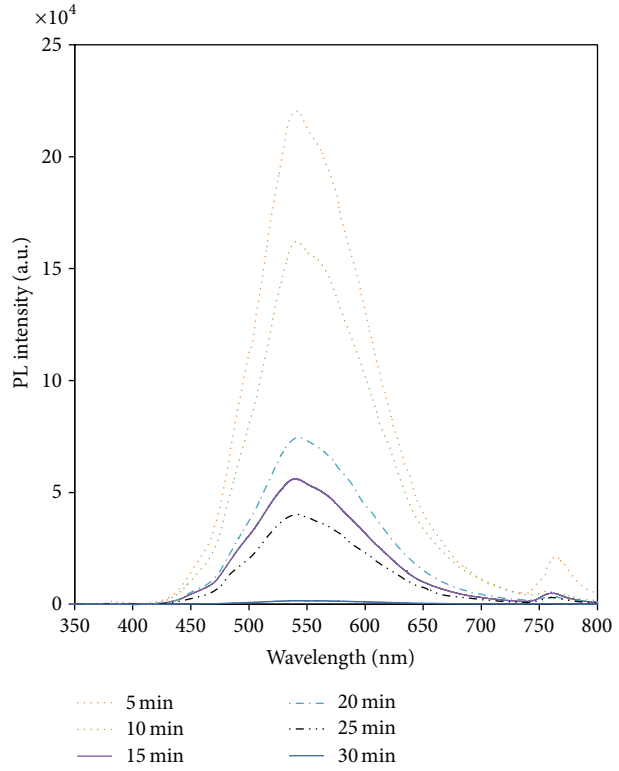

Figure 5: Photoluminescence profile of ZnO NWs deposited at various growth times of 5, 10, 15, 20, 25, and 30 minutes.

Blue region around 460 nm (2.70 eV) can be linked to the presence of complexes of zinc interstitials (Zn_i) [23].

The broad DLE green emissions at ~540 nm (2.29 eV) can be related to oxygen vacancies (Vo) [20]. Halliburton et al. have shown that DL green emission is due to shallow donors or conduction band electrons [24]. Zhang et al. [25] and Patterson [26] have proved that Vo is an unlikely contributor to green emission compared to zinc vacancies (V_{Zn}^{2-}) based on the electron transition state. V_{Zn}^{2-} has the lowest formation energy in O-rich conditions and in our experiment this is prevalent as the growth time was increased. The use of methanol environment provided excess oxygen for the ZnO formation reactions. Thus, V_{Zn}^{2-} is the most

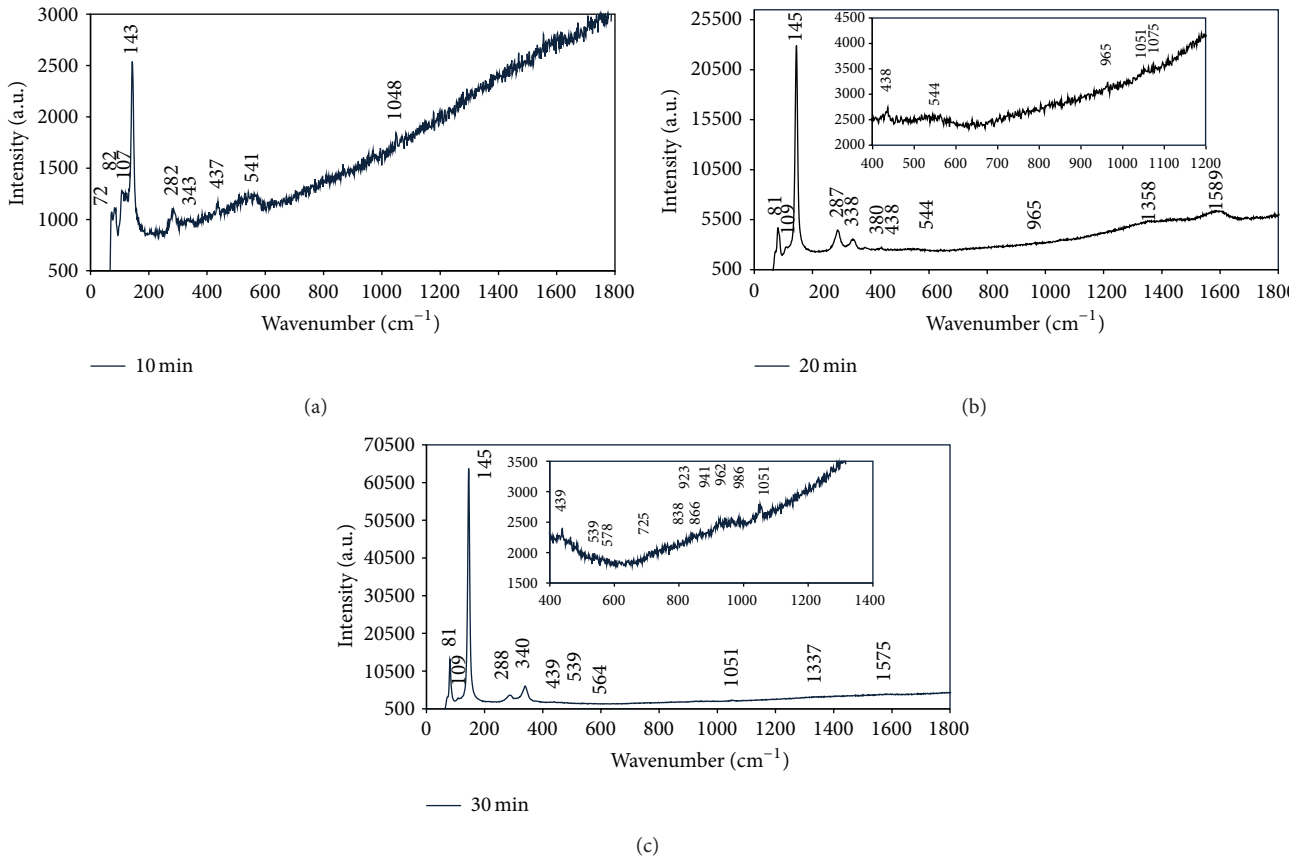

Figure 6: Raman scattering of ZnO NWs prepared at growth times of (a) 10, (b) 20, and (c) 30 minutes.

Table 2: Details of photoluminescence peaks of ZnO NWs near band edge, deep level, and infrared emissions obtained from Gaussian fits.

Deposition time (minutes)	NBE		DL		NIR	
	Peak position (cm^{-1})	Energy (eV)	Peak position (cm^{-1})	Energy (eV)	Peak position (cm^{-1})	Energy (eV)
5 minutes	382	3.24	541	2.29	764	1.62
10 minutes	381	3.25	541	2.28	761	1.62
15 minutes	381	3.25	540	2.29	761	1.63
20 minutes	382	3.24	540	2.29	762	1.62
25 minutes	381	3.25	540	2.28	762	1.63
30 minutes	378	3.28	541	2.28	755	1.64

energetically favorable and stable defects in the synthesized ZnO nanorods [25].

Small broad shoulder ~560 nm (2.21 eV) indicates emissions of yellowish-green band from all ZnO NWs samples prepared at growth times of 5, 10, 15, 20, 25 and 30 minutes. This can be related to shallow donor H+ defects in the ZnO nanorods which presents from the methanol solution [27]. ZnO NWs are believed to be a good candidate to study doping levels in ZnO nanostructures. The observed yellow luminescence at ~560 nm (2.20 eV) is attributed to recombination of donors with acceptors from methanol solution believed to be H acceptors. Near infrared (NIR) luminescence ~762 nm was observed in all ZnO samples except for sample prepared at growth time of 30 minutes which shows NIR at 755 nm.

3.4. Raman Scattering. Figures 6(a), 6(b), and 6(c) show Raman spectrum of ZnO NWs which were prepared at growth times of 10, 20, and 30 minutes. Dominant peak at 143 cm^{-1} is noticeable in ZnO NWs deposited at growth time of 10 minutes, whereas dominant peak at 145 cm^{-1} is observable in ZnO NWs of growth times of 20 and 30 minutes. The intensity at 143 cm^{-1} was found to be enhanced as the growth time of ZnO NWs was increased by 10 minutes at constant substrate temperature of 800°C. Cuscò et al. also have observed the same peak and have reported that intensity enhancement and sharpening of the peak at 142 cm^{-1} as Raman scattering was done at lower temperatures at 80 K due to local mode origin of the peak. This is in contradiction to our room temperatures Raman scattering [28].

Two peaks at lower wavenumber around 72 and 82 cm^{-1} were noticed in ZnO NWs of all samples. It is found to be peaks 72 and 82 cm^{-1} splitting from a single peak for lower growth time of 10 minutes. As the growth time was increased to 20 and 30 minutes peak at 72 cm^{-1} diminished and the peak at 82 cm^{-1} was found to be sharper. A research team from Germany has reported that this Raman peak at 82 cm^{-1} is related to bare ZnO nanoparticles obtained by decomposing Zn oximate in dimethyl formamide (DMF) [29]. The same group also has reported that Raman peak at 105 cm^{-1} can be assigned to ZnO/MWCNT which is similar to peaks 107 and 109 cm^{-1} which were obtained in the sample of ZnO NWs prepared for growth times of 10, 20, and 30 minutes. The similarity in observation attributes incorporation of carbon particles to ZnO NWs. The observed peaks at ~82, ~109, ~143, and ~282 cm^{-1} which are below 300 cm^{-1} can be related to vibrations of Zn sublattice. Peak ~282 cm^{-1} that has A_1 symmetry can be assigned to B_1^{high}-B_1^{low} mode. This peak was shifted to 287 and 288 cm^{-1} as the growth time increased to 20 and 30 minutes, respectively.

At the intermediate low frequency region the E_2^{high} mode at 437, 438, and 439 cm^{-1} is noticeable, respectively, in samples prepared at growth times of 10, 20, and 30 minutes. These peaks were found to be sharper as the growth time was increased. This is an indication of O stoichiometry completion for longer growth time whereby Zn particles were bonded to O to form ZnO NWs. Peaks 343, 338, and 340 cm^{-1} which has A_1 symmetry are observable, respectively, in ZnO NWs prepared at growth times of 10, 20, and 30 minutes. These modes are in good agreement with the difference between E_2^{high} and E_2^{low} frequencies. However, 343 cm^{-1} was observed to be broaden due to split up into 82 and 107 cm^{-1} frequency.

Peak at 380 cm^{-1} is observable only in ZnO NWs which was prepared in 20 minutes. This peak reflects A_1(TO) mode measured to be in the room temperature Raman scattering. This contradicted to Cusco et al. of spectrum that has recorded the peak only at 80 K of Raman scattering. A broad band in region 500-600 cm^{-1} found to be diminished as the growth time was increased from 10 to 30 minutes. It is broadening with centered at 541 cm^{-1} for ZnO NWs prepared at growth time of 10 minutes. This can be assigned to A_1 symmetry and attributed to $2B_1^{low}$ and LA overtones along L, M, and H lines. As the broadening is diminished relatively to the increased growth time, extra peaks at 564 and 578 cm^{-1} were noticed. As in Figure 6(b) only one extra peak at 564 cm^{-1} is noticeable for ZnO NWs of 20 minutes while two peaks at 564 and 578 cm^{-1} are detectable for ZnO NWs prepared at growth time of 30 minutes. Peak 564 cm^{-1} can be revealed to nonresonance Raman scattering, whereas 578 cm^{-1} which is close to A_1(LO) mode has been reported by Ye et al. [30] in resonance Raman spectra of ZnO quantum dots. This peak in the proximity of A_1(LO) was assigned to surface optical modes predicted theoretically and O vacancies, Zn interstitials, or combination of the two [31].

High frequency region from 820–1120 cm^{-1} has been reported that formed by optical overtones and combinations of TO and LO [32]. A weak peak at 1048 cm^{-1} which is observable in ZnO NWs of 10 minutes can be assigned TO+LO combination modes at the A and H points. As the growth time was increased to 20 and 30 minutes the peak has been shifted to right to 1051 cm^{-1}. In sample ZnO NWs of 30 minutes, the peak was found to be sharper with high intensity. Additionally, a peak at 1075 and 1090 cm^{-1} only on ZnO NWs of 20 and 30 minutes is noticeable. This peaks can be assigned to be TO+LO combination modes at M and L points. ZnO NWs of 20 and 30 minutes of growth time show first order Raman absorption for the disordered bands D and G. A weak shoulder band D at 1358 and 1337 cm^{-1} was found in sample prepared at growth times of 20 and 30 minutes, respectively. The G band appeared to be broader compared to the D band. The G bands around 1589 and 1575 cm^{-1} are observable, respectively, in ZnO NWs of 20 and 30 minutes. As the growth time was increased from 20 to 30 minutes both the D and G bands were shifted to left. The presence of D and G band clearly indicated the presence of graphitic carbon in the sample. The C formed during the synthesis process was due to C particles from methanol vapor.

3.5. TEM. The TEM images of the ZnO NWs are shown in Figure 7. An assortment of nanostructures mainly NWs and nanoplates is observable in Figure 7(a). High resolution imaging of a selected NW in Figure 7(a), shown here in Figure 7(b), revealed clear crystal lattice fringes and the estimated distance between adjacent lattice planes was 0.26 nm. This corresponded to the (0002) plane which indicated that the selected ZnO NWs were grown in the *c*-axis direction.

3.6. Growth Mechanism. A series of chemical mechanisms were proposed based on various outcomes that have been established elsewhere [33]. The thermally heated CuZn alloy has allowed only Zn atoms to escape as Zn vapors at temperatures greater than 395°C which then condensed into Zn solid on Si substrate. Here the presence of Ar environment believed has played an important role in changing the morphology of Zn film from large boundary to nanosized grain [34]. We also believe that the presence of Ar at 100 sccm in the isolated system thermodynamically has rearranged and reduced the crystallite size of hexagonal ZnO

$$\mathrm{ZnCu\,(solid\ brass)} \xrightarrow{>395^{\circ}\mathrm{C}} \mathrm{Zn\,(vapor)} \longrightarrow \mathrm{Zn\ film.} \tag{2}$$

The growth of ZnO NWs in Figure 2 is obtained by allowing methanol vapor as Ar was flowed at 100 sccm through the mixture of methanol and acetone solution via two-sided hollow CuZn. We believed that C, H, and O atoms in methanol underwent a dehydrogenation process in the presence of Cu (in CuZn alloy) at 300°C.

$$\begin{aligned} \mathrm{CH_3OH_{(a)}} &\xrightarrow{\mathrm{Cu,300^{\circ}C}} \mathrm{CH_3O_{(a)}} + \mathrm{H_{(a)}} \\ \mathrm{CH_3O_{(a)}} &\xrightarrow{\mathrm{Cu,300^{\circ}C}} \mathrm{HCHO_{(a)}} + \mathrm{H_{(a)}}. \end{aligned} \tag{3}$$

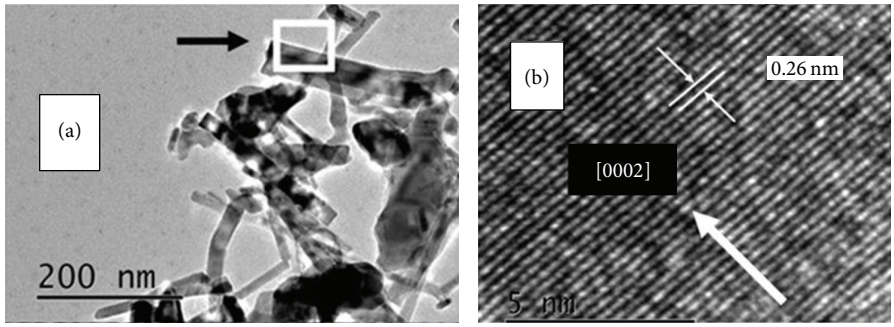

Figure 7: TEM images of ZnO NWs (a) at low resolution and (b) at high resolution.

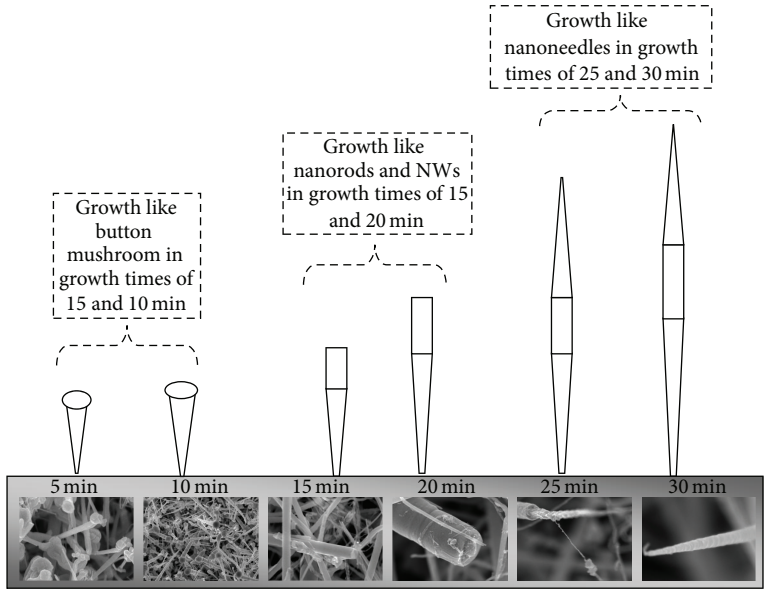

Figure 8: Predicted time dependent growth mechanism for ZnO NWs as growth time varies from 5 to 30 minutes.

Based on that, Cu in CuZn has acted as an catalyst and has oxidized the methanol vapor into an intermediate absorbable methoxy species ($CH_3O_{(a)}$) and hydrogen atom ($H_{(a)}$) [35]. The $CH_3O_{(a)}$ is thermodynamically unstable and was readily converted to formaldehyde (HCHO) by releasing a $H_{(a)}$. The higher bond energy of C=O in HCHO is thermodynamically unfavorable and the polarity of carbonyl group and its high basicity lowered the transition state energy of activation and therefore results in faster rate of reaction with readily presence species [36]. So the chemically unstable HCHO vapor easily reacts with Zn vapor or Zn atoms to that which have been thermally evaporated at temperatures above 395∘C to form hexagonal ZnO NWs. Besides that, further oxidation of HCHO to HCOOH is not predicted due to O_2 absence environment.

Apart from this, C–O bond in $CH_3O_{(a)}$ was readily cleaved by Zn vapors [37]. Coadsorption of $O_{(a)}$ and $Zn_{(a)}$ appeared to give rise to reactive oxygen ions (O^{2-}) and Zn ions (Zn^{2+}) on the Si substrate. Thus Zn^{2+} ionically bonds with O^{2-} to form ZnO nanostructures

$$CH_3O_{(a)} \longrightarrow O_{(a)} + CH_{3(a)}$$

$$\begin{aligned} O_{(a)} + 2e^- &\longrightarrow O^{2-} \\ Zn_{(a)} + O^{2-} &\longrightarrow ZnO\,(\text{nanowires})\,. \end{aligned} \tag{4}$$

Based on the results and images of ZnO NWs prepared at different growth time of 5–30 minutes in steps of 5 minutes depicts controversial growth mechanisms that have not been reported elsewhere. Figure 8 shows an illustration of proposed growth mechanism. Structural transformation during the time-dependent growth of ZnO NWs has been taken into account. The shape has changed from button mushroom to NWs/nanorods and to nanoneedles as the growth time was increased from 5 minutes to 30 minutes. At growth time of 20 minutes growth of nanoneedles from a base of ~150 nm diameter of ZnO is noticeable. A ZnO nanostring seems to be connected between the nanoneedle and ZnO flakes. At the growth time of 30 minutes formation of nanoneedles was observed to be in a cone shape.

4. Conclusion

VPT of methanol and thermal evaporation of CuZn assisted with hotwire is a feasible technique that can be utilized in

synthesizing hexagonal ZnO NWs in the laboratory. ZnO NWs in hexagonal shape is produced with crystalline size of 23.6 nm for growth time of 5 minutes. Formation of ZnO nanostrings and NWs was confirmed as the growth time was increased to 25 and 30 minutes. Calculated crystalline size shows independency on increased growth time where a drop in crystalline size after 25 minutes of growth period is noticeable. Although the intensity in the PL profile is inversely proportional to increased growth time V_{Zn}^{2-} is likely a contributor in the green emission region. Yellow emission region related recombination of donors to H+ defects sides. Blue region around 460 nm (2.70 eV) confirmed presence of complexes of Zn_i. Raman peaks also confirmed decoration of the wall of ZnO NWs with C particles from methanol. Interlattice spacing of 0.26 nm showed growth of ZnO NWs in (0002) direction.

In future studies the ZnO NWs produced using other aliphatic alcohols can be considered promising material in future applications. This is due to possible functionalization on ZnO NWs using C source materials.

Conflict of Interests

The authors declare that there is no conflict of interests regarding the publication of this paper.

Acknowledgment

This work is supported by Peruntukan Penyelidikan Pasca-siswazah (PPP) of University Malaya Grant no. PS212/2009A and UMRG Grant no. RG247-12AFR.

References

[1] C. Jagadish and S. J. Pearton, *Zinc Oxide Bulk, Thin Films, and Nanostructures: Processing, Properties, and Applications*, Elsevier, Amsterdam, The Netherlands, 2006.

[2] M. Guo, P. Diao, and S. M. Cai, "Photoelectrochemical properties of highly oriented ZnO nanotube array films on ITO substrates," *Chinese Chemical Letters*, vol. 15, no. 9, pp. 1113–1116, 2004.

[3] R. D. Piner, J. Zhu, F. Xu, S. Hong, and C. A. Mirkin, "'Dip-pen' nanolithography," *Science*, vol. 283, no. 5402, pp. 661–663, 1999.

[4] G. Y. Yi, C. Wang, and W. I. Park, "ZnO nanorods: synthesis, characterization and applications," *Semiconductor Science and Technology*, vol. 20, supplement 4, pp. S22–S34, 2005.

[5] Z. Lockman, Y. Pet Fong, T. Wai Kian, K. Ibrahim, and K. A. Razak, "Formation of self-aligned ZnO nanorods in aqueous solution," *Journal of Alloys and Compounds*, vol. 493, no. 1-2, pp. 699–706, 2010.

[6] C. S. Lao, J. Liu, P. Gao et al., "ZnO nanobelt/nanowire schottky diodes formed by dielectrophoresis alignment across au electrodes," *Nano Letters*, vol. 6, no. 2, pp. 263–266, 2006.

[7] S. Kim, M. C. Jeong, B. Y. Oh, W. Lee, and J. M. Myoung, "Fabrication of Zn/ZnO nanocables through thermal oxidation of Zn nanowires grown by RF magnetron sputtering," *Journal of Crystal Growth*, vol. 290, no. 2, pp. 485–489, 2006.

[8] L. Wang, K. Chen, and L. Dong, "Synthesis of exotic zigzag ZnO nanoribbons and their optical, electrical properties," *Journal of Physical Chemistry C*, vol. 114, no. 41, pp. 17358–17361, 2010.

[9] W. Ouyang and J. Zhu, "Catalyst-free synthesis of macro-scale ZnO nanonail arrays on Si substrate by simple physical vapor deposition," *Materials Letters*, vol. 62, no. 17-18, pp. 2557–2560, 2008.

[10] S. L. Wang, X. Jia, P. Jiang, H. Fang, and W. H. Tang, "Large-scale preparation of chestnut-like ZnO and Zn–ZnO hollow nanostructures by chemical vapor deposition," *Journal of Alloys and Compounds*, vol. 502, no. 1, pp. 118–122, 2010.

[11] Q. J. Feng, L. Z. Hu, H. W. Liang et al., "Catalyst-free growth of well-aligned arsenic-doped ZnO nanowires by chemical vapor deposition method," *Applied Surface Science*, vol. 257, no. 3, pp. 1084–1087, 2010.

[12] P. Tonto, O. Mekasuwandumrong, S. Phatanasri, V. Pavarajarn, and P. Praserthdam, "Preparation of ZnO nanorod by solvothermal reaction of zinc acetate in various alcohols," *Ceramics International*, vol. 34, no. 1, pp. 57–62, 2008.

[13] Y. S. Lim, J. W. Park, S.-T. Hong, and J. Kim, "Carbothermal synthesis of ZnO nanocomb structure," *Materials Science and Engineering B: Solid-State Materials for Advanced Technology*, vol. 129, no. 1–3, pp. 100–103, 2006.

[14] C. Jia, Y. Chen, G. Liu, X. Liu, S. Yang, and Z. Wang, "Growth of c-oriented ZnO films on (0 0 1) SrTiO3 substrates by MOCVD," *Journal of Crystal Growth*, vol. 311, no. 1, pp. 200–204, 2008.

[15] A. Wagner, A. Behrends, A. Waag, and A. Bakin, "Two step deposition method with a high growth rate for ZnO nanowire arrays and its application in photovoltaics," *Thin Solid Films*, vol. 520, no. 14, pp. 4637–4641, 2012.

[16] D. Yu, T. Trad, J. T. McLeskey Jr., V. Craciun, and C. R. Taylor, "ZnO nanowires synthesized by vapor phase transport deposition on transparent oxide substrates," *Nanoscale Research Letters*, vol. 5, no. 8, pp. 1333–1339, 2010.

[17] Z. Zhu, T.-L. Chen, Y. Gu, J. Warren, and R. M. Osgood Jr., "Zinc oxide nanowires grown by vapor-phase transport using selected metal catalysts: a comparative study," *Chemistry of Materials*, vol. 17, no. 16, pp. 4227–4234, 2005.

[18] A. Baruj, P. A. Larochette, S. Sommadossi, and H. E. Troiani, "Surface phase transformation induced by the dezincification of a beta Cu–Zn alloy on highly deformed systems," *Applied Surface Science*, vol. 254, no. 1, pp. 72–75, 2007.

[19] X. L. Chen, X. H. Geng, J. M. Xue, D. K. Zhang, G. F. Hou, and Y. Zhao, "Temperature-dependent growth of zinc oxide thin films grown by metal organic chemical vapor deposition," *Journal of Crystal Growth*, vol. 296, no. 1, pp. 43–50, 2006.

[20] K. Vanheusden, W. L. Warren, C. H. Seager, D. R. Tallant, J. A. Voigt, and B. E. Gnade, "Mechanisms behind green photoluminescence in ZnO phosphor powders," *Journal of Applied Physics*, vol. 79, no. 10, pp. 7983–7990, 1996.

[21] M. H. Huang, Y. Wu, H. Feick, N. Tran, E. Weber, and P. Yang, "Catalytic growth of zinc oxide nanowires by vapor transport," *Advanced Materials*, vol. 13, no. 2, pp. 113–116, 2001.

[22] D. M. Bagnall, Y. F. Chen, Z. Zhu, T. Yao, M. Y. Shen, and T. Goto, "High temperature excitonic stimulated emission from ZnO epitaxial layers," *Applied Physics Letters*, vol. 73, no. 8, pp. 1038–1040, 1998.

[23] D. C. Look, G. C. Farlow, P. Reunchan, S. Limpijumnong, S. B. Zhang, and K. Nordlund, "Evidence for native-defect donors in n-type ZnO," *Physical Review Letters*, vol. 95, no. 22, Article ID 225502, pp. 2–4, 2005.

[24] L. E. Halliburton, N. C. Giles, N. Y. Garces et al., "Production of native donors in ZnO by annealing at high temperature in Zn vapor," *Applied Physics Letters*, vol. 87, no. 17, Article ID 172108, pp. 1–3, 2005.

[25] S. Zhang, S.-H. Wei, and A. Zunger, "Intrinsic *n*-type versus *p*-type doping asymmetry and the defect physics of ZnO," *Physical Review B*, vol. 63, Article ID 075205, pp. 1–7, 2001.

[26] C. Patterson, "Role of defects in ferromagnetism in Zn1—xCoxO: a hybrid density-functional study," *Physical Review B*, vol. 74, Article ID 144432, pp. 1–13, 2006.

[27] C. G. van de Walle, "Hydrogen as a doping cause in ZnO," *Physical Review Letters*, vol. 85, pp. 1012–1015, 2000.

[28] R. Cuscò, E. Alarcón-Lladó, J. Ibáñez et al., "Temperature dependence of Raman scattering in ZnO," *Physical Review B*, vol. 75, Article ID 165202, pp. 1–11, 2007.

[29] J. Khanderi, R. C. Hoffmann, A. Gurlo, and J. J. Schneider, "Synthesis and sensoric response of ZnO decorated carbon nanotubes," *Journal of Materials Chemistry*, vol. 19, no. 28, pp. 5039–5046, 2009.

[30] J. D. Ye, S. Tripathy, F. Ren, X. W. Sun, G. Q. Lo, and K. L. Teo, "Raman-active Fröhlich optical phonon mode in arsenic implanted ZnO," *Applied Physics Letters*, vol. 94, no. 1, Article ID 011913, pp. 1–3, 2009.

[31] S. Baskoutas, P. Giabouranis, S. N. Yannopoulos et al., "Preparation of ZnO nanoparticles by thermal decomposition of zinc alginate," *Thin Solid Films*, vol. 515, no. 24, pp. 8461–8464, 2007.

[32] J. Serrano, A. H. Romero, F. J. Manjón, R. Lauck, M. Cardona, and A. Rubio, "Pressure dependence of the lattice dynamics of ZnO: an ab initio approach," *Physical Review B-Condensed Matter and Materials Physics*, vol. 69, no. 9, Article ID 94306, pp. 1–14, 2004.

[33] L. S. Panchakarla, A. Govindaraj, and C. N. R. Rao, "Formation of ZnO nanoparticles by the reaction of zinc metal with aliphatic alcohols," *Journal of Cluster Science*, vol. 18, no. 3, pp. 660–670, 2007.

[34] H. Lv, D. D. Sang, H. D. Li, X. B. Du, D. M. Li, and G. T. Zou, "Thermal evaporation synthesis and properties of ZnO nano/microstructures using carbon group elements as the reducing agents," *Nanoscale Research Letters*, vol. 5, no. 3, pp. 620–624, 2010.

[35] A. K. Chen and R. Masel, "Direct conversion of methanol to formaldehyde in the absence of oxygen on Cu(210)," *Surface Science*, vol. 343, no. 1-2, pp. 17–23, 1995.

[36] P. Y. Bruice, *Organic Chemistry*, 5th edition, 2006.

[37] K. R. Harikumar and C. N. R. Rao, "Role of oxygen transients in the facile scission of C–O bonds of alcohols on Zn surfaces," *Chemical Communications*, no. 4, pp. 341–342, 1999.